Article

The Application of Barocaloric Solid-State Cooling in the Cold Food Chain for Carbon Footprint Reduction

Luca Cirillo [ID], Adriana Greco [ID] and Claudia Masselli *[ID]

Department of Industrial Engineering, University of Naples Federico II, P.le Tecchio 80, 80125 Naples, Italy; luca.cirillo2@unina.it (L.C.); adriana.greco@unina.it (A.G.)
* Correspondence: claudia.masselli@unina.it

Abstract: In this paper, the application of solid-state cooling based on the barocaloric effect in the cold food supply chain is investigated. Barocaloric solid-state technology is applied to the final links of the cold food supply chain regarding the steps of retail and domestic conservation. In this context, effective barocaloric cooling entails the refrigeration of food at 5 °C (273 K) and as such is a promising cooling technology due to its energy efficiency and environmental friendliness. The categories of food involved in this investigation are meat and fresh food products like soft cheese, yogurt, and milk. The energy performance of the barocaloric system is analyzed and compared with a commercial vapor compression refrigerator of a similar size, both operating using R600a under the same working conditions. Based on the results of this comparison, it is concluded that barocaloric cooling is a favorable technology for application in the final links of the cold food supply chain if the system operates in an ABR cycle at frequencies between 1.25 and 1.50 Hz with a regenerator comprising acetoxy silicone rubber as the solid-state refrigerant and a 50%EG–50% water mixture as the heat transfer fluid flowing at an optimal velocity of 0.15 m s^{-1}. Thus, an appropriate tradeoff between the temperature span, cooling power, and coefficient of performance is guaranteed. Under these conditions, the barocaloric system outperforms the domestic vapor compression cooler operating using R600a.

Keywords: barocaloric; food supply chain; carbon footprint reduction; solid-state cooling; energy saving

1. Introduction

In the last decade, the global community has fully grasped the risk of climate change and has started implementing countermeasures to slow its effects. Environmental sustainability has become essential for any new technological innovation; the objective is to fully realize sustainable development goals as soon as possible. One of the most significant contributors to environmental pollution is greenhouse gas emissions from air conditioning systems [1,2] in buildings and industrial warehouses, as well as coupled systems for refrigeration [3,4]. Therefore, the design and management of these systems must increasingly consider strict emission guidelines [5].

Over the years, and considering the increasing health consciousness among consumers, the food industry has evolved significantly to meet high market demand and maintain high-quality standards.

The aspect that links the refrigeration and air-conditioning sector and the food industry is the cold food chain [6]. The expression "cold chain" indicates the maintenance of fresh and frozen products at a constant temperature throughout their life cycle, from the production plant to the point of sale, through all transport and storage stages. Maintaining food storage temperature helps to ensure that the product obtained by the consumer is intact, without having undergone thermal shocks that could alter the organoleptic properties of the food. The goal is to prevent the cold chain from being interrupted in one of the supply chain stages, compromising the product's nutritional properties and posing a threat to its integrity, hygiene standards, and food safety [7].

Since a temperature that is too high or too low might negatively impact the food's quality and/or safety, each food product has a defined ideal storage temperature. Refrigeration is used at every stage of the food supply chain, from food processing to distribution, retail sales, and final consumption. Various cooling methods and strict temperature control during different processes are crucial to ensure the target production levels are reached, and the product's organoleptic qualities are kept consistent at every production stage. Reliable, efficient, sustainable, and high-quality production processes are needed to meet the requirements for reduced energy use and effective energy management. According to the findings from the High-Level Panel of Experts on Food Security and Nutrition, the concept of food systems encompasses various elements like food production, supply networks, environments, dietary habits, and consumer selection [8]. It also considers the resulting impacts on nutrition, the environment, and socioeconomic aspects. The processes and phases associated with the production, processing, distribution, marketing, consumption, and disposal of food all fall under the scope of food supply chains, which are becoming progressively intricate. The proportion of global greenhouse gas emissions attributed to the overall food system, encompassing activities beyond the retail stage like cooking and waste disposal, is projected to rise significantly if the food and agriculture sector continues to account for roughly a quarter (26%) of worldwide greenhouse gas emissions (amounting to 34% of total greenhouse gases) [9,10]. While the primary production phase undoubtedly makes the largest contribution, subsequent activities within the supply chain such as processing, transportation, packaging, and retail collectively contribute to 18% of greenhouse gas emissions related to food. Notably, emissions resulting from food waste are substantial, accounting for approximately one-quarter of emissions (equivalent to 3.3 billion tons of CO2eq) generated during food production. These emissions occur due to inefficiencies in the supply chain (contributing to 15% of food-related greenhouse gases) as well as consumer losses [11].

To ensure competitiveness in the global market while simultaneously reducing environmental impacts, the food sector must minimize its energy consumption and increase the use of ecofriendly facilities [12]. In terms of achieving all these goals, optimizing refrigeration/freezing systems represents a significant challenge [13]. European food hygiene and safety regulations provide detailed guidelines concerning the temperatures required for food preservation. Regulation EC No. 852/04 [14] states that food businesses handling perishable products must have all the necessary facilities to maintain the "cold chain" for these products. Suitable structures such as refrigerated rooms, freezers, and (or) display counters must be available for the storage and display of perishable goods. However, all these measures alone are insufficient, as different food products must be kept at specific temperatures that must be continuously monitored. Therefore, the equipment must be designed to allow for temperature control and recording.

In general, however, the legal provisions on this matter are quite elaborate and also refer to different storage periods: transportation, warehousing, and display [15,16]. Traditional food preservation devices exhibit evident limitations in terms of environmental sustainability. Specifically, most refrigeration systems currently rely on the vapor compression cycle [17,18]. Over the years, the development of this technology has faced significant challenges in terms of the environmental impact associated with the use of refrigerants, many of which have proven to be highly detrimental to the environment, both in terms of damaging the planet's stratospheric ozone layer and contributing to global warming.

In this context, research increasingly considers alternatives to traditional vapor compression systems: On the one end of the spectrum, there are renewable-energy-based technologies such as solar [19–22] or geothermal [23–26] technologies, while on the other, there are solid-state technologies based on the caloric effect [27–30]. These alternatives do not use refrigerant gases, thus ensuring a negligible contribution to the greenhouse effect [31]. They also have potentially higher performance coefficients than vapor compression systems, leading to energy savings of 50–60%, no noise during operation, and easy

maintenance [32–35]. These technologies fully align with the global political context aiming to reduce greenhouse gas emissions and transition towards a low-carbon economy.

The operating principle of solid-state systems is the caloric effect: It occurs when a caloric material is subjected to an external field that induces a temperature change by varying its intensity under adiabatic conditions (ΔT_{ad}). If the field varies under isothermal conditions, an entropy change (ΔS_{iso}) can be observed in the material [36–38]. Depending on the nature of the applied external field and the thermophysical properties of the caloric material, specific caloric effects can be achieved: magnetocaloric (magnetic field) [39], electrocaloric (electric field) [40,41], and mechanocaloric (mechanical stress) [42–46]. The caloric effect is divided into two types depending on the applied external field. If the external field is generated due to mechanical stress, such as compression [47], tension [48], or torsion [49], it is called the elastocaloric effect [50,51]. This effect occurs in specific materials known as shape memory alloys [52–54]. On the other hand, if the applied field is the result of hydrostatic pressure, it is referred to as the barocaloric effect [55,56].

Recently, there has been a growing interest in the solid-state cooling effect known as barocaloric [57]. As a result, there are relatively fewer scientific publications with respect to other techniques related to caloric effects [58]. The interest in barocaloric effects emerged when studies suggested that magnetocaloric materials undergoing first-order phase transitions might experience a temperature change under adiabatic pressure variation [59].

Various investigations were conducted, and some years later, it was experimentally confirmed that many materials exhibiting magnetocaloric properties also show the possibility of detecting the barocaloric effect. Moreover, it was found that the barocaloric effect could be coupled with other caloric effects, leading to multicaloric effects in the same material. Another promising class of barocaloric materials includes elastomer natural rubbers.

Researchers like Moya et al. have provided comprehensive reviews [58,59] on barocaloric materials. However, the number of barocaloric materials that have been developed and investigated for cooling applications continuously increases. Besides materials, the research on the development of devices for cooling applications also lacks experimental results derived from the operation of barocaloric prototype devices. To the best of our knowledge, in 2014, Czernuszewicz et al. proposed the concept of a magnetobarocaloric test stand for cooling applications [60], which, similar to their previously developed magnetocaloric test stand [61], allows for assessing the application potential of materials that exhibit temperature changes under the influence of magnetization and applied pressure.

In 2018, Aprea et al. conducted a comprehensive study on caloric materials used in an active caloric cooler, including some of the most promising barocaloric refrigerants [62]. This investigation provided an up-to-date overview of their energy performance, establishing a general framework for these materials.

One significant outcome of the study above is the confirmation that barocaloric cooling holds great promise and is comparable to vapor compression (VC) cooling. Selecting promising barocaloric materials for cooling applications is crucial to developing efficient active barocaloric coolers. Additionally, the use of more efficient auxiliary fluids is necessary to ensure that this technique is environmentally friendly. Typically, water or a water–glycol mixture is used as the auxiliary fluid, depending on whether the caloric system operates above or below zero degrees Celsius.

Thus, the aim of this investigation is to study the application of barocaloric solid-state technology to the final links of the cold food supply chain, for retail and domestic food storage. In this context, we tested a barocaloric cooler for keeping food at 5 °C (273 K), to evaluate the potential of this method as a promising, energy-efficient, and environmentally friendly cooling technology. The food categories of interest were meat and fresh food products (soft cheese, yogurt, and milk).

In summary, the main objectives of this research are as follows:

- We aim to examine the energy efficiency of a solid-state barocaloric cooling system designed to function as a refrigeration machine for selling cold products, which need

to be kept at 278 K. The scenario is assumed to be a hot indoor environment to examine the potentialities of this technology in extreme summer conditions (313 K). Our purpose is to compare its performance with the performance of an existing vapor compression refrigerator commonly used in industrial settings. The solid-state system involves active barocaloric regeneration, using a heat-transfer fluid consisting of a 50% ethylene glycol (EG) and 50% water mixture, while the solid-state refrigerant is acetoxy silicone rubber (ASR) [63–66].

- We aim to assess and compare the energy efficiency of the active barocaloric cycle with that of a commercial vapor compression refrigerator of a similar size, both operating under the same working conditions.

2. The Project "PNRR on Foods" and the Cold Chain

The research investigation presented in this paper is part of the maxi-project PNRR "ONFOODS" research activities. The concept of sustainability has only recently entered everyday use. Sustainability refers to patterns of production and consumption that respect natural resources and their usual rhythms, focusing on long-term resilience and avoiding the depletion of resources and environmental degradation.

The 2030 Agenda for Sustainable Development, adopted by all United Nations Member States in 2015, describes 17 Sustainable Development Goals (SDGs), ranging from ending poverty to improving health and education, reducing inequality, spurring economic growth, tackling climate change, and working to preserve our oceans and forests.

The project ONFOODS (Research and Innovation Network on Food and Nutrition Sustainability, Safety, and Security—Working on Foods) is financed by the European Community and is among the activities of the Italian PNRR, i.e., the National Recovery and Resilience Plan (PNRR). This plan is part of the Next Generation EU (NGEU) program, a EUR 750 billion package, accounting for about half of the grants agreed upon by the European Union in response to the pandemic crisis of 2020. Within this framework, ONFOODS is an action plan with a comprehensive approach, joining together and synergizing the strengths and competencies of several different disciplines, ranging from social and juridical sciences to agricultural economics, food chemistry, food technology and engineering, logistics, microbiology, marketing, human nutrition, and many disciplines of medicine. Only through a holistic approach can we preserve the environment, develop strategies for the effective implementation of our food systems, and, at the same time, improve the well-being of individuals and extend their healthy life span by reducing avoidable and premature mortality and inequity and putting people at the center of a more effective, safe, sustainable, and fair social security system.

ONFOODS faces this challenge through a coordinated action involving seven spokes, each one focusing on a very specific, although broad, aspect of food production, transformation, and effect. All these spokes will be deeply intertwined in a complex and well-developed network of connections and complementation, where ideas that originate in one spoke will become innovation only after being validated in the work of researchers collaborating in other relevant spokes within the program.

The identified objectives of ONFOODS are as follows:

- To promote the sustainability of food production;
- To increase the adherence to more sustainable dietary patterns;
- To promote the sustainability of food distribution;
- To increase the quality of foods and diets;
- To develop smart innovative technologies for sustainable food production and consumption;
- To guarantee food safety and food security at the whole population level and in specific vulnerable targets of the population.

The research group of the University of Naples Federico II, to which the authors belong, is focused on the ONFOODS activities to "promote the sustainability of food distribution", i.e., to potentiate the sustainability of the cold chain in all its steps.

The cold chain begins with production; it continues through the storage phase in refrigerated platforms, followed by the transport phase up to the sales warehouses and refrigerated counters of the points of sale, and ends with the final consumers' coolers. Every step is essential for the success of the cold chain process. More details are provided in Figure 1, which illustrates the phases of the food cold supply chain.
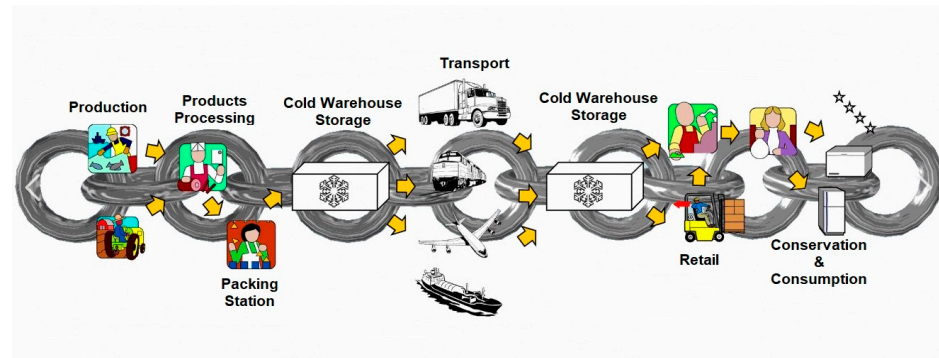

Figure 1. The phases of the food cold supply chain.

I.   Production and Product Processing: Upon leaving the packaging lines, measuring the core temperature of the product is necessary to determine the time required to reach the temperature indicated on the packages. After physical–chemical and bacteriological assessments, thermosensitive food products—fresh or frozen—are managed under refrigeration and stored in temperature-controlled warehouses.

II.   Cold Warehouse Storage: The storage of food products in cold rooms guarantees an overall reduction in their core temperature, and the picking and order preparation activities can also be carried out in the same environment. Based on the type of product, it must also be ensured that the ideal temperatures and hygienic conditions of containers and packaging are maintained; loading areas must also be under a controlled temperature and possibly adjacent to the logistics cell.

III.   Transport: This phase is of crucial importance for the cold chain. In fact, vehicles must be equipped with refrigerators already at the required temperature, which should be maintained during transport to another facility for cold storage or the points of sale of large-scale retail trade. This occurs through the use of tools that allow operators to keep the air temperature in the compartment under control.

IV.   Retail: Products are displayed in retail outlets on special refrigerated shelves and are available for purchase by the consumer.

Conservation and Consumption: After purchasing food products, the consumer keeps them in their refrigerators until they are used for consumption.

During all these steps of the cold chain, in order to avoid any contamination, operators are required to meticulously implement and monitor the following features:

- The cleanliness and hygienic conditions of warehouses, equipment, and transport;
- The pre-established critical limits in various stages of the cold chain;
- The temperatures of the different actors of the cold chain.

In this context, Spoke 3 of ONFOODS (Research and Innovation Network on Food and Nutrition Sustainability, Safety, and Security—Working on Foods) has the following objectives:

- To report on best storage and operational solutions for food waste control and reduction in energy consumption;
- To focus on the use of phase change materials (PCMs) for the steps of the cold chain process related to (II) cold warehouse storage and (III) transport;
- To apply ecofriendly technologies as an alternative to vapor compression for refrigeration systems used in the steps related to (IV) retail and (V) conservation and consumption.

Temperature-sensitive products must therefore follow precise hygienic measures and comply with the temperatures required by law. As suggested by Italian Legislative Decree 27 January 1992, n.110 [67], frozen foods must maintain a constant temperature of $-18°$ Celsius; however, during transport, brief upward swings not exceeding 3 °C are allowed. As far as fresh food is concerned, however, each one has its own reference temperature:

- Meats: +5 °C to +7 °C;
- Fish: +2 °C;
- Fresh products: +5 °C;
- Ice creams: -22 °C;
- Chocolate: +18 °C to +20 °C.

Following the description of Spoke 3 of PNRR ONFOODS, this investigation aims to introduce barocaloric solid-state technology as an alternative to vapor compression for the links of the cold food supply chain related to retail and domestic conservation. The food categories of interest in this investigation are meat and fresh food products (soft cheese, yogurt, and milk), kept at 5 °C (273 K) using an energy-efficient and environmentally friendly barocaloric cooler. The system is tested while operating in a hot indoor environment to examine the potentialities of the technology in extreme summer conditions (313 K). The method is also compared with the vapor compression technology.

3. The Thermodynamic Cycle Based on the Barocaloric Effect

Active barocaloric refrigeration involves an active barocaloric regenerative cycle in which a barocaloric material serves as the refrigerant. The system consists of a barocaloric regenerator housed in a pressure cell to enable variations in the working pressure. This regenerator interacts with cold and hot heat exchangers, and a heat transfer fluid is used to facilitate the heat exchange while passing through the barocaloric material. The regenerator can be designed in various ways, such as using porous media, parallel plates, or wires of the barocaloric material, creating channels through which the auxiliary fluid flows, among other possibilities.

Figure 2 illustrates an example of the active barocaloric regenerative refrigeration cycle using a parallel plate design. It is essential to clarify that the purpose of Figure 2 is to conceptually depict the four processes of the active barocaloric regenerative refrigeration cycle from a thermodynamic standpoint rather than presenting a detailed engineering design. The ABR cycle comprises two isobaric and two adiabatic processes, as evident in Figure 2a.

With reference to Figure 2b, during the first process (Step I), the barocaloric regenerator undergoes adiabatic loading, increasing hydrostatic pressure from p_0 to p_1. This results in a temperature rise in the barocaloric material due to the BCE (transformation 1–2 of Figure 2a). Once the pressure reaches p_1, the loading process ends, and the system exchanges heat with the hot heat exchanger through the heat transfer fluid (HTF) flow (Step II of Figure 2b). Consequently, as depicted in the transformation 2–3 of Figure 2a, the ABR starts to decrease in temperature. Subsequently, Step III (Figure 2b) involves adiabatic unloading, with the pressure decreasing from p_1 to p_0, which causes the further cooling of the ABR, as shown in transformation 3–4 in Figure 2a.

Lastly, as seen in Step IV (Figure 2b), the HTF flowing in the ABR results in heat being subtracted from the cold heat exchanger, thus achieving the desired cooling effect. Consequently, the regenerator undergoes an increase in temperature (transformation 4-1 of Figure 2a).
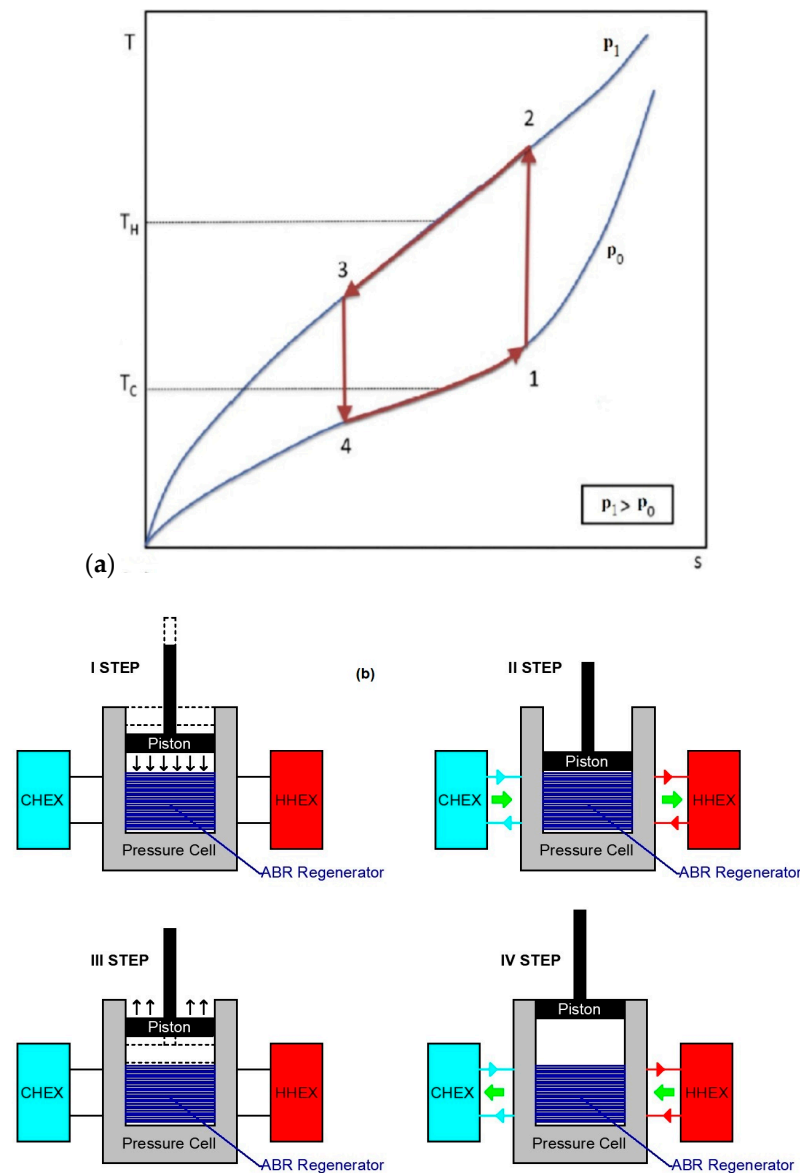
Figure 2. The Brayton-based ABR cycle: (**a**) on T–s diagram; (**b**) applied to the cooling system.

3.1. The Barocaloric Material

The selection of an appropriate barocaloric substance for cooling applications is influenced by the range of the desired operating temperature and the specific intended use. To be considered a promising refrigerant for caloric cooling, a material must meet several essential criteria, such as affordability, ease of synthesis, and non-toxicity [68]. Moreover, the material must exhibit significant adiabatic temperature changes (ΔT_{ad}) within the designated temperature range. With these objectives in mind, we opted to utilize acetoxy silicone rubber (ASR) [63] in our investigation, as it is a widely available, cost-effective, and environmentally friendly elastomer. ASR is a type of elastomer that belongs to the vulcanizing rubber category, and its thermophysical properties are reported in Table 1.

Table 1. Thermophysical properties of acetoxy silicone rubber.

Material	Thermal Conductivity (W m^{-1} K^{-1})	Density (kg m^{-3})	Adiabatic Temperature Change (K) at $\Delta p = 0.390$ GPa
ASR	1.48	960	41.1

One of the key characteristics of this group of materials is their remarkable elasticity: These vulcanizing rubber materials can be repeatedly stretched to their original length when subjected to relatively low pressures. This ability makes them noteworthy as potential mechanocaloric materials, as they combine their elastomeric properties with promising structural transitions. Acetoxy silicone rubber, composed of polydimethylsiloxane, additives, and illers, demonstrates an extraordinary barocaloric effect, displaying a significant ΔT_{ad} peak during crystalline (41.1 K) to amorphous transitions, which leads to rearrangements of the polymer chains. As shown in Figure 3, Imamura et al. [63] generated a diagram for the change in the adiabatic temperature of acetoxy silicone rubber during the decompression process at a pressure of Δp = 0.390 GPa, plotted against the working temperature of the material at the start of the transformation. The complete details of the measurements and the methodology utilized can be found in a previous study [63]. The peak barocaloric effect occurs at approximately 41.1 K, near 298 K. Considering a suitable working temperature range for domestic refrigeration purposes (278 ÷ 313 K), the observed values of ΔT_{ad} remain above 30 K, affirming the applicability of ASR for this type of cooling application. ASR is classified as a vulcanizing rubber material, and there is a significant concern regarding its fatigue behavior. Researchers such as Sebald et al. [68] investigated the impact of fatigue behavior on the degradation of barocaloric properties, while Woo et al. [69] developed a tool for predicting fatigue life. The findings by Sebald et al. [68] indicate that the barocaloric effect (BCE) temperature degradation is much lower than the magnitude of stress degradation. On the other hand, Woo et al. [69] observed that the fatigue failure of such materials typically occurs after approximately 6×10^5 cycles (in the order of magnitude).
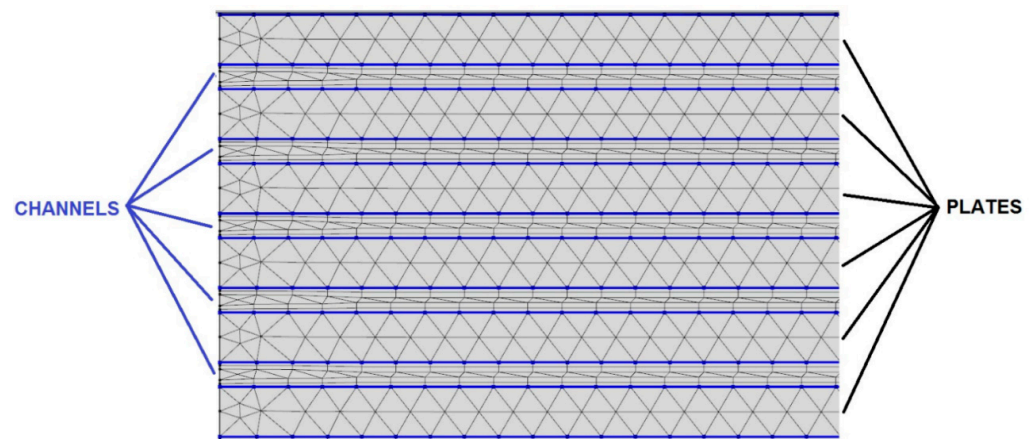

Figure 3. An image of the regenerator's triangular mesh is utilized to solve the model.

3.2. Mathematical Modeling

This analysis was conducted utilizing a 2D model of an ABR refrigerator. The regenerator (measuring 20 mm × 45 mm) was constructed with 54 parallel plates made of barocaloric substances, enabling HTF (heat transfer fluid) flow for exchanging heat with the hot and cold heat exchangers. The thickness of every plate was 0.25 mm, whereas the distance stacked between two consecutive plates, i.e., the height of the channel where the auxiliary fluid flows, was 0.125 mm.

Before introducing the model, the following assumptions should be noted:

- Laminar is the regime of motion of the auxiliary fluid.
- The auxiliary fluid is considered incompressible.
- The viscous dissipation is neglected since the mass flow is small.
- The fluid direction is modeled through a velocity that has a positive sign if the fluid flows from the cold to the hot heat exchanger and a negative sign for fluid flowing from the hot to the cold heat exchanger.

- The presence of the cold and hot heat exchangers is ensured by the Dirichlet boundary conditions driving the model during the fluid flow steps (temperature of the cold heat exchanger if the fluid flows from cold to hot; temperature of the hot heat exchanger if the fluid flows from hot to cold side).

The mathematical framework governing the four processes of the ABR cycle is outlined as follows (Navier–Stokes equations and the equation of the energy for the fluid and the solid [70]):

$$
\begin{cases}
\frac{\partial u}{\partial x} + \frac{\partial v}{\partial y} = 0 \\
\frac{\partial u}{\partial t} + u\frac{\partial u}{\partial x} + v\frac{\partial u}{\partial y} = -\frac{1}{\rho_f}\frac{\partial p}{\partial x} + v\left(\frac{\partial^2 u}{\partial x^2} + \frac{\partial^2 u}{\partial y^2}\right) \\
\frac{\partial v}{\partial t} + u\frac{\partial v}{\partial x} + v\frac{\partial v}{\partial y} = -\frac{1}{\rho_f}\frac{\partial p}{\partial y} + v\left(\frac{\partial^2 v}{\partial x^2} + \frac{\partial^2 v}{\partial y^2}\right) \\
\frac{\partial T_f}{\partial t} + u\frac{\partial T_f}{\partial x} + v\frac{\partial T_f}{\partial y} = \frac{k_f}{\rho_f C_f}\left(\frac{\partial^2 T_f}{\partial x^2} + \frac{\partial^2 T_f}{\partial y^2}\right) \\
\rho_s C\frac{\partial T_s}{\partial t} = k_s\left(\frac{\partial^2 T_s}{\partial x^2} + \frac{\partial^2 T_s}{\partial y^2}\right) + Q
\end{cases}
\tag{1}
$$

where u and v are the components of the fluid velocity vector along the x and y axes; p is the fluid pressure; and T_f and T_s are the fluid and solid temperatures, respectively. k, ρ, and C are the thermal conductivity, density, and heat capacity of the fluid (if they are coupled with the f subscript) or of the solid (if they are followed by the s subscript).

In Steps I and III of the ABR cycle, the fluid is not moving, and the elastocaloric effect occurs through $+Q$ and $-Q$, respectively; thus, Equation (1) becomes

$$
\begin{cases}
\rho_f C_f\frac{\partial T_f}{\partial t} = k_f\left(\frac{\partial^2 T_f}{\partial x^2} + \frac{\partial^2 T_f}{\partial y^2}\right) \\
\rho_s C\frac{\partial T_s}{\partial t} = k_s\left(\frac{\partial^2 T_s}{\partial x^2} + \frac{\partial^2 T_s}{\partial y^2}\right) + Q
\end{cases}
\tag{2}
$$

with

$$
Q = Q(field, T_S) = \frac{\rho_s\, C(field, T_s)\Delta T_{ad}(field, T_s)}{\tau}
\tag{3}
$$

The Q functions were derived using specialized software that identifies the closest mathematical representation to the input table function. These functions were generated based on experimental data previously published in the literature. Table 2 contains the mathematical expressions corresponding to the various investigated pressure loads. To solve the equations of the model, the finite element method was employed, and the regenerator underwent meshing using the free triangular meshing approach (depicted in Figure 3).

Table 2. $Q\ast\tau$ functions, related to the field increasing process, obtained starting from the experimental data.

Material	Δp (GPa)	Mathematical Expression
ASR	0.390	$Q_{load}\ast\tau = 10^6 \ast$ $\left[(1.33\ast T + 0.000211\ast\left(T^2\ast sin(4.33 + sin(-0.0636\ast T)\ast sin(4.12 + sin(0.0726\ast T) - 165 - 0.00216\ast T)\right]\right.$

The concept was previously presented in one of our earlier investigations and experimentally validated through accurate comparison with experimental data obtained using a rotary permanent magnet magnetocaloric cooler prototype, a collaborative project developed by the University of Naples Federico II and the University of Salerno [39,62]. In fact, one of the key characteristics of our model is its ability to accurately simulate the behavior of an active regenerator with the use of any solid-state refrigerant, regardless of the particular caloric impact displayed.

The finite element method (FEM) is employed to solve the model, while the ABR cycle is an iterative process, repeating multiple times until reaching a steady-state condition that fulfills the cutoff criterion at every point of the ABR regenerator:

$$\delta = max\{T(x, y, 0 + n\theta) - T(x, y, 4\tau + n\theta)\} < \bar{\varepsilon} \tag{4}$$

4. Thermal Performance Analysis

The ABR regenerator utilizes acetoxy silicone rubber as the barocaloric refrigerant, with Δp = 0.390 GPa during the adiabatic compression–decompression process. This study was conducted with specific parameters set at a temperature range of 278 ÷ 313 K, where the lower and upper limits represent the cold and hot heat exchanger temperatures, respectively. Each ABR cycle had a total duration of 0.8 s, with each step lasting 0.2 s. The Heat transfer fluid employed in the system was a mixture of 50% ethylene glycol (EG) and 50% water, with a whole freezing point of 236 K.

Table 3 summarizes the parameters and ranges used in this investigation.

Table 3. Operating conditions of the numerical investigation.

Parameter	Unit	Value
$T_{set\ point}$	K	278
f	Hz	1.25
Δp	GPa	0.390
v	m s^{-1}	0.04–0.2

The most significant parameters characterizing the energy performances were determined as follows:

$$\Delta T_{span} = T_H - \frac{1}{\tau} \int_{3\tau+q\theta}^{4\tau+q\theta} T_f(0, y, t) dt \tag{5}$$

where ΔT_{span} is the temperature span measured across the regenerator during the last process of the ABR cycle in steady-state conditions.

$$\dot{Q}_{ref} = \frac{1}{\theta} \int_{3\tau+q\theta}^{4\tau+q\theta} \dot{m}_f C_f \left(T_C - T_f(0, y, t) \right) dt \tag{6}$$

where $\dot{Q}_{ref}$ is the proper refrigeration power of the ABR refrigerator.

$$COP = \frac{\dot{Q}_{ref}}{\dot{W}_{TOT}} = \frac{\dot{Q}_{ref}}{\dot{W}_{field} + \dot{W}_{pump}} \tag{7}$$

where the *COP* (coefficient of performance) measures the cooling power of the refrigerator relative to the combined expenses involved in its operation. W_{TOT} represents the contribution of changes in the external field (W_{field}) and the mechanical power needed to move the heat transfer fluid (W_{pump}).

To evaluate the energy efficiency of the barocaloric refrigerator, its energy performance was compared with the experimental results obtained from a standard food cooler operating under identical conditions. This allowed for a reference point to gauge the level of performance attained by the solid-state system.

5. Results

In this section, the energy performance of the elastocaloric device is evaluated when functioning in the cooling mode. The graph in Figure 4 illustrates that the variation in the temperature span, represented as ΔT_{span}, consistently exceeds 35 K. This is an essential

parameter for evaluating the performance of a thermal device, such as the elastocaloric device introduced in the previous section. A wide temperature span indicates a higher capacity to transfer heat and provide cooling or heating effects. At a speed of 0.10 m s^{-1} and a frequency of 1.5 Hz, the maximum ΔT_{span} value reaches 39.2 K. It is interesting to note that there are two distinct regions in the graph. In the low-speed zone, the temperature increases, while in the high-speed zone, the temperature decreases. This effect is mainly due to the exchange time between fluid and barocaloric material; as the speed increases, the exchange time between fluid and material decreases, not allowing the thermal flow to fully undergo the exchange process. Therefore, there is an optimum air velocity for each frequency beyond which the temperature span values decrease.
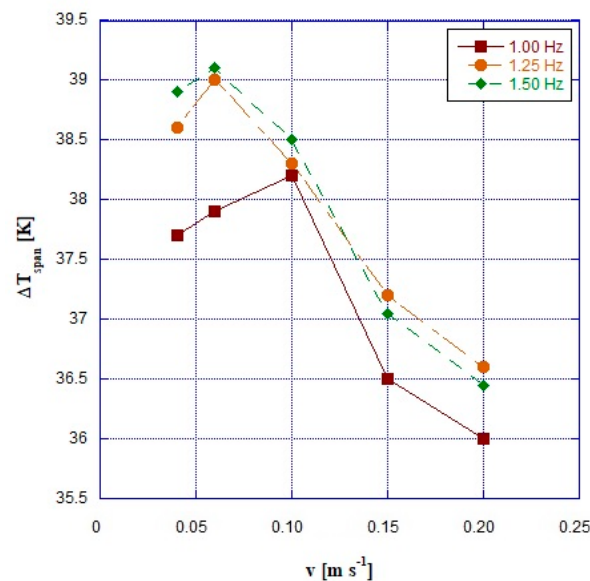
Figure 4. Temperature span as a function of the fluid velocity for different frequencies of the ABR cycle.

The specific cooling capacity of the barocaloric system is shown in Figure 5 as a function of fluid flow velocity. We compared the proposed system with a vapor compression cooler, which is a Samsung RB38T705CB1 VC system using 62.5 g of R600a.
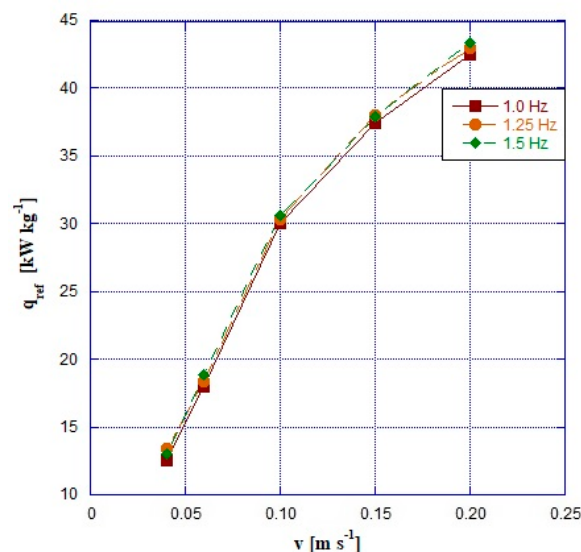

Figure 5. Specific cooling power as a function of the fluid velocity for different frequencies of the ABR cycle.

The VC system has a 1 kW cooling capacity and is intended for household use. The system's cooling capacity per kilogram is 16 kW kg^{-1}. Figure 5 shows that the barocaloric system outperforms the vapor compression system for fluid velocities greater than 0.06 m s^{-1}. The specific cooling power of the barocaloric system is always greater than the conventional system for HTF velocities greater than 0.05 m s^{-1}. At a frequency of 1.5 Hz and a speed of 0.20 m s^{-1}, it reaches its maximum value of 44 kW kg^{-1}.

The fluctuations in the coefficient of performance (COP) with HTF velocity at different frequencies are shown in Figure 6. The most favorable COP readings are observed at a frequency of 1.25 Hz and an HTF velocity of 0.20 m s^{-1}, reaching a peak value of approximately 4.5. Even the standard vapor-compression-based system achieves highly satisfactory *COP* values.
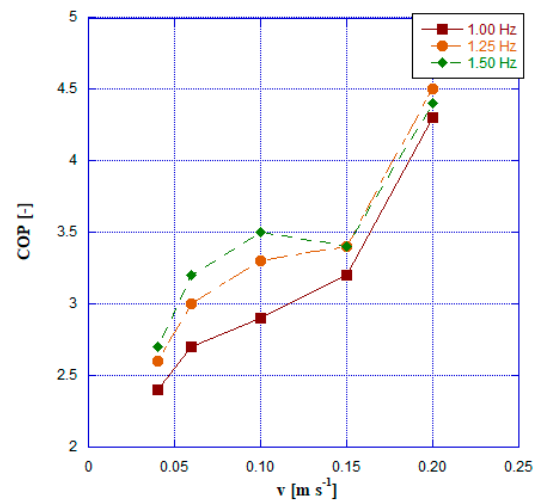
Figure 6. Coefficient of performance as a function of the fluid velocity for different frequencies of the ABR cycle.

Figure 7 demonstrates the results of the *COP* comparison between a residential refrigerator based on vapor compression and a barocaloric cooler. The following equation was used to obtain the comparison data:

$$\frac{\Delta COP}{COP} = \frac{COP_{ABR} - COP_{VC}}{COP_{VC}} \tag{8}$$

As shown in Figure 7, the velocity values of the HTF equal to or greater than 0.15 m s^{-1} always ensure energy savings if the domestic cooler is based on the ABR cycle. If the velocity is 0.10 m s^{-1}, the frequencies of 1.25 and 1.50 ensure a positive gain in terms of *COP*. The results demonstrate that the ABR cycle consistently outperforms the traditional vapor compression refrigerator, with up to 40% improvement. For low-velocity values and all frequencies, the barocaloric system does not achieve the same *COP* values as the traditional system. However, for velocities higher than 0.06 m s^{-1}, the barocaloric device manages to achieve improvements of over 40% for all frequencies.
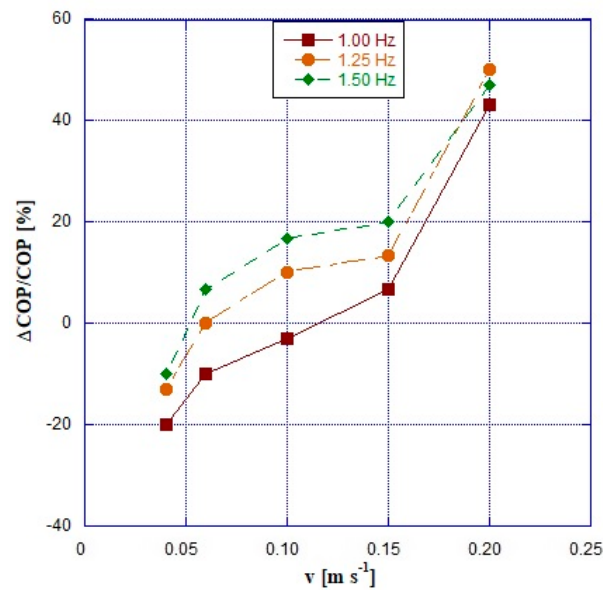
Figure 7. Coefficient of performance of the barocaloric cooler compared with that of a domestic vapor compression cooler.

6. Conclusions

In this research, the energy efficiency analysis of an active barocaloric refrigerator intended to serve cold food storage is presented. Using a 2D tool based on the finite element approach, we assessed its energy performance, considering factors like temperature span, cooling power, mechanical power, and coefficient of performance. The system was tested while operating in a hot indoor environment to examine the potentialities of the technology in extreme summer conditions (313 K). The food categories of interest in this investigation were meat and fresh food products (soft cheese, yogurt, and milk), kept at 5 °C (278 K) using a barocaloric cooler, which is considered an energy-efficient and environmentally friendly system. The features of Spoke 3 of PNRR ONFOODS were also used to compare the proposed method with vapor compression technology. In this investigation, vapor compression was replaced with barocaloric solid-state technology for the steps of the cold food supply chain associated with retail and household food preservation. The barocaloric system runs on an active barocaloric regenerative refrigeration cycle, with acetoxy silicone rubber serving as the solid-state refrigerant and ethylene glycol serving as HTF. From this investigation, the following conclusions can be drawn:

- The temperature span always exceeds 35 K, and it reaches a peak of 39.2 at a speed of 0.10 m s^{-1} and a frequency of 1.5 Hz.
- For fluid velocity greater than 0.06 m s^{-1}, the barocaloric system outperforms the vapor compression system in terms of cooling power. The peak of 44 kW kg^{-1} is reached at a speed of 0.20 m s^{-1} and a frequency of 1.5 Hz.
- The most favorable COP readings are observed at a frequency of 1.25 Hz and an HTF velocity of 0.20 m s^{-1}, reaching a peak value of approximately 4.5.
- Velocity values of the HTF equal to or greater than 0.15 m s^{-1} always ensure energy savings if the domestic cooler is based on the ABR cycle.

Based on the following considerations, it is concluded that barocaloric cooling is a favorable technology to employ in the final links of the cold food supply chain if the system operates with the ABR cycle at frequencies between 1.25 and 1.50 Hz with a regenerator comprising acetoxy silicone rubber as the solid-state refrigerant and 50%EG–50%water mixture as the heat transfer fluid flowing at the optimal velocity of 0.15 m s^{-1}. This solution guarantees an appropriate tradeoff between the temperature span, the cooling power, and the coefficient of performance. Under these conditions, the barocaloric system outperforms the domestic vapor compression cooler operating with R600a.

Nomenclature

Roman symbols

c	Specific heat capacity, J kg^{-1} K^{-1}
COP	Coefficient of performance, -
f	Frequency, Hz
k	Thermal conductivity, W m^{-1} K^{-1}
L	The whole length of the system, mm
n	Number of times
p	Pressure, Pa
$\dot{Q}$	Power density due to caloric effect, W m^{-3}
q	Thermal power density, W m^{-2}
S	Entropy, J kg K
T	Temperature, K
t	Time, s
u	Longitudinal velocity coordinate, m s^{-1}
V	Volume, m^3
v	Orthogonal velocity coordinate, m s^{-1}
x	Longitudinal spatial coordinate, m
X	Conjugate field
y	Orthogonal spatial coordinate, m
Y	Driving field

Greek symbols

Δ	Finite difference
δ	Infinitesimal difference
ρ	Density, kg m^{-3}

Subscripts

ad	Adiabatic
C	Cold heat exchanger
cycle	Cycle
f	Fluid
H	Hot heat exchanger

p	Constant pressure
ref	Refrigeration
s	Solid

References

1. Benhadid-Dib, S.; Benzaoui, A. Refrigerants and their environmental impact Substitution of hydro chlorofluorocarbon HCFC and HFC hydro fluorocarbon. Search for an adequate refrigerant. *Energy Procedia* **2012**, *18*, 807–816. [CrossRef]
2. Aprea, C.; Greco, A. An exergetic analysis of R22 substitution. *Appl. Therm. Eng.* **2002**, *22*, 1455–1469.
3. Aprea, C.; Greco, A.; Rosato, A. Comparison of R407C and R417A heat transfer coefficients and pressure drops during flow boiling in a horizontal smooth tube. *Energy Convers. Manag.* **2008**, *49*, 1629–1636.
4. Llopis, R.; Torrella, E.; Cabello, R.; Sánchez, D. HCFC-22 replacement with drop-in and retrofit HFC refrigerants in a two-stage refrigeration plant for low temperature. *Int. J. Refrig.* **2012**, *35*, 810–816.
5. United Nation Environment Program. *Montreal Protocol on Substances that Deplete the Ozone Layer*; United Nation Environment Program (UN): New York, NY, USA, 1987.
6. James, S.J.; James, C.J.F.R.I. The food cold-chain and climate change. *Food Res. Int.* **2010**, *43*, 1944–1956.
7. Mercier, S.; Villeneuve, S.; Mondor, M.; Uysal, I. Time–temperature management along the food cold chain: A review of recent developments. *Compr. Rev. Food Sci. Food Saf.* **2017**, *16*, 647–667. [PubMed]
8. Audsley, E.; Brander, M.; Chatterton, J.C.; Murphy-Bokern, D.; Webster, C.; Williams, A.G. How low can we go? An assessment of greenhouse gas emissions from the UK food system and the scope reduction by 2050. In *Report for the WWF and Food Climate Research Network*; WWF-UK: London, UK, 2010.
9. Garnett, T. Where are the best opportunities for reducing greenhouse gas emissions in the food system (including the food chain)? *Food Policy* **2011**, *36*, S23–S32.
10. Oenema, O.; Velthof, G.; Kuikman, P. Technical and policy aspects of strategies to decrease greenhouse gas emissions from agriculture. *Nutr. Cycl. Agroecosyst.* **2001**, *60*, 301–315.
11. Camanzi, L.; Alikadic, A.; Compagnoni, L.; Merloni, E. The impact of greenhouse gas emissions in the EU food chain: A quantitative and economic assessment using an environmentally extended input-output approach. *J. Clean. Prod.* **2017**, *157*, 168–176.
12. Cascetta, F.; Di Lorenzo, R.; Nardini, S.; Cirillo, L. A Trnsys Simulation of a Solar-Driven Air Refrigerating System for a Low-Temperature Room of an Agro-Industry site in the Southern part of Italy. *Energy Procedia* **2017**, *126*, 329–336. [CrossRef]
13. Aprea, C.; de Rossi, F.; Greco, A.; Renno, C. Refrigeration plant exergetic analysis varying the compressor ca-pacity. *Int. J. Energy Res.* **2003**, *27*, 653–669. [CrossRef]
14. Regulation (EC) No 852/2004 of The European Parliament and of the Council. 2004.
15. Zhang, Y.; Xu, Y.; Lu, R.; Zhang, S.; Hai, A.M.; Tang, B. Form-stable cold storage phase change materials with durable cold insulation for cold chain logistics of food. *Postharvest Biol. Technol.* **2023**, *203*, 112409. [CrossRef]
16. Bozorgi, M.; Roy, P.; Siddique, A.R.M.; Venkateshwar, K.; Tasnim, S.; Mahmud, S. Experimental investigation and life cycle assessment of a phase change material (PCM) based thermoelectric (TE) refrigerator. *Int. J. Thermofluids* **2023**, *19*, 100394. [CrossRef]
17. Aprea, C.; Greco, A.; Vanoli, G. Condensation heat transfer coefficients for R22 and R407C in gravity driven flow regime within a smooth horizontal tube. *Int. J. Refrig.* **2003**, *26*, 393–401.
18. Aprea, C.; Rossi, F.; Greco, A. Experimental evaluation of R22 and R407C evaporative heat transfer coefficients in a vapour compression plant. *Int. J. Refrig.* **2000**, *23*, 366–377. [CrossRef]
19. Jiao, C.; Li, Z. An Updated Review of Solar Cooling Systems Driven by Photovoltaic–Thermal Collectors. *Energies* **2023**, *16*, 5331.
20. Alahmer, A.; Ajib, S. Solar cooling technologies: State of art and perspectives. *Energy Convers. Manag.* **2020**, *214*, 112896.
21. Otanicar, T.; Taylor, R.A.; Phelan, P.E. Prospects for solar cooling–An economic and environmental assessment. *Sol. Energy* **2012**, *86*, 1287–1299.
22. Hwang, Y.; Radermacher, R.; Al Alili, A.; Kubo, I. Review of solar cooling technologies. *HvacR Res.* **2008**, *14*, 507–528. [CrossRef]
23. D'agostino, D.; Esposito, F.; Greco, A.; Masselli, C.; Minichiello, F. Parametric analysis on an earth-to-air heat exchanger employed in an air conditioning system. *Energies* **2020**, *13*, 2925. [CrossRef]
24. D'Agostino, D.; Esposito, F.; Greco, A.; Masselli, C.; Minichiello, F. The energy performances of a ground-to-air heat exchanger: A comparison among köppen climatic areas. *Energies* **2020**, *13*, 2895. [CrossRef]
25. Greco, A.; Masselli, C. The optimization of the thermal performances of an earth to air heat exchanger for an air conditioning system: A numerical study. *Energies* **2020**, *13*, 6414. [CrossRef]
26. Ketfi, O.; Abdi, H.; Lounici, B.; Bourouis, M. Performance Analysis of Low-Capacity Water–LiBr Absorption–Cooling Systems Using Geothermal Heat-Sinks in Hot Climates. *Energies* **2023**, *16*, 809. [CrossRef]
27. Fähler, S.; Rößler, U.K.; Kastner, O.; Eckert, J.; Eggeler, G.; Emmerich, H.; Entel, P.; Müller, S.; Quandt, E.; Albe, K. Caloric effects in ferroic materials: New concepts for cooling. *Adv. Eng. Mater.* **2012**, *14*, 10–19. [CrossRef]
28. Vopson, M.M.; Fetisov, Y.K.; Hepburn, I. Solid-state heating using the multicaloric effect in multiferroics. *Magnetochemistry* **2021**, *7*, 154. [CrossRef]

29. Garcia-Ben, J.; Delgado-Ferreiro, I.; Salgado-Beceiro, J.; Bermudez-Garcia, J.M. Simple and low-cost footstep energy-recover barocaloric heating and cooling device. *Materials* **2021**, *14*, 5947. [CrossRef] [PubMed]

30. Kabirifar, P.; Žerovnik, A.; Ahčin, Ž.; Porenta, L.; Brojan, M.; Tušek, J. Elastocaloric cooling: State-of-the-art and future challenges in designing regenerative elastocaloric devices. *Stroj. Vestn./J. Mech. Eng.* **2019**, *65*, 615–630. [CrossRef]

31. Aprea, C.; Greco, A.; Maiorino, A.; Masselli, C. The employment of caloric-effect materials for solid-state heat pumping. *Int. J. Refrig.* **2020**, *109*, 1–11. [CrossRef]

32. Alahmer, A.; Al-Amayreh, M.; Mostafa, A.O.; Al-Dabbas, M.; Rezk, H. Magnetic refrigeration design technologies: State of the art and general perspectives. *Energies* **2021**, *14*, 4662. [CrossRef]

33. Silva, D.J.; Ventura, J.; Araújo, J.P. Caloric devices: A review on numerical modeling and optimization strategies. *Int. J. Energy Res.* **2021**, *45*, 18498–18539. [CrossRef]

34. Takeuchi, I.; Sandeman, K. Solid-state cooling with caloric materials. *Phys. Today* **2015**, *68*, 48–54. [CrossRef]

35. Bachmann, N.; Schwarz, D.; Bach, D.; Schäfer-Welsen, O.; Koch, T.; Bartholomé, K. Modeling of an Elastocaloric Cooling System for Determining Efficiency. *Energies* **2022**, *15*, 5089. [CrossRef]

36. Fähler, S.; Pecharsky, V.K. Caloric effects in ferroic materials. *MRS Bull.* **2018**, *43*, 264–268. [CrossRef]

37. Kitanovski, A.; Plaznik, U.; Tomc, U.; Poredoš, A. Present and future caloric refrigeration and heat-pump technologies. *Int. J. Refrig.* **2015**, *57*, 288–298. [CrossRef]

38. Moya, X.; Mathur, N.D. Caloric materials for cooling and heating. *Science* **2020**, *370*, 797–803. [CrossRef] [PubMed]

39. Aprea, C.; Greco, A.; Maiorino, A.; Masselli, C. Analyzing the energetic performances of AMR regenerator working with different magnetocaloric materials: Investigations and viewpoints. *Int. J. Heat Technol.* **2017**, *35*, S383–S390. [CrossRef]

40. Greco, A.; Masselli, C. Electrocaloric cooling: A review of the thermodynamic cycles, materials, models, and devices. *Magnetochemistry* **2020**, *6*, 67. [CrossRef]

41. Li, Q.; Shi, J.; Han, D.; Du, F.; Chen, J.; Qian, X. Concept design and numerical evaluation of a highly efficient rotary electrocaloric refrigeration device. *Appl. Therm. Eng.* **2021**, *190*, 116806. [CrossRef]

42. Engelbrecht, K. Future prospects for elastocaloric devices. *J. Phys. Energy* **2019**, *1*, 021001. [CrossRef]

43. Ismail, M.; Yebiyo, M.; Chaer, I. A review of recent advances in emerging alternative heating and cooling technologies. *Energies* **2021**, *14*, 502. [CrossRef]

44. Chen, J.; Lei, L.; Fang, G. Elastocaloric cooling of shape memory alloys: A review. *Mater. Today Commun.* **2021**, *28*, 102706. [CrossRef]

45. Porenta, L.; Trojer, J.; Brojan, M.; Tušek, J. Experimental investigation of buckling stability of superelastic Ni-Ti tubes under cyclic compressive loading: Towards defining functionally stable tubes for elastocaloric cooling. *Int. J. Solids Struct.* **2022**, *256*, 111948. [CrossRef]

46. Lloveras, P.; Tamarit, J.-L. Advances and obstacles in pressure-driven solid-state cooling: A review of barocaloric materials. *MRS Energy Sustain.* **2021**, *8*, 3–15. [CrossRef]

47. Chen, J.; Zhang, K.; Kan, Q.; Yin, H.; Sun, Q. Ul-tra-high fatigue life of NiTi cylinders for compression-based elastocaloric cooling. *Appl. Phys. Lett.* **2019**, *115*, 093902. [CrossRef]

48. Tušek, J.; Engelbrecht, K.; Mikkelsen, L.P.; Pryds, N. Elastocaloric effect of Ni-Ti wire for application in a cooling device. *J. Appl. Phys.* **2015**, *117*, 124901. [CrossRef]

49. Wang, R.; Fang, S.; Xiao, Y.; Gao, E.; Jiang, N.; Li, Y.; Mou, L.; Shen, Y.; Zhao, W.; Li, S.; et al. Torsional Refrigeration by Twisted, Coiled, and Supercoiled Fibers. Available online: http://science.sciencemag.org/ (accessed on 30 July 2023).

50. Greibich, F.; Schwödiauer, R.; Mao, G.; Wirthl, D.; Drack, M.; Baumgartner, R.; Kogler, A.; Stadlbauer, J.; Bauer, S.; Arnold, N.; et al. Elastocaloric heat pump with specific cooling power of 20.9 W g–1 exploiting snap-through instability and strain-induced crystallization. *Nat. Energy* **2021**, *6*, 260–267. [CrossRef]

51. Cirillo, L.; Farina, A.R.; Greco, A.; Masselli, C. Numerical optimization of a single bunch of niti wires to be placed in an elastocaloric experimental device: Preliminary results. *Magnetochemistry* **2021**, *7*, 67. [CrossRef]

52. Ahčin, Ž.; Kabirifar, P.; Porenta, L.; Brojan, M.; Tušek, J. Numerical modeling of shell-and-tube-like elastocaloric regenerator. *Energies* **2022**, *15*, 9253. [CrossRef]

53. Ma, S.; Zhang, X.; Zheng, G.; Qian, M.; Geng, L. Toughening of Ni-Mn-Based Polycrystalline Ferromagnetic Shape Memory Alloys. *Materials* **2023**, *16*, 5725. [CrossRef]

54. Zhu, Y.; Tsuruta, R.; Gupta, R.; Nam, T. Feasibility Investigation of Attitude Control with Shape Memory Alloy Actuator on a Tethered Wing. *Energies* **2023**, *16*, 5691. [CrossRef]

55. Cirillo, L.; Greco, A.; Masselli, C. Cooling through barocaloric effect: A review of the state of the art up to 2022. *Therm. Sci. Eng. Prog.* **2022**, *33*, 101380. [CrossRef]

56. Aprea, C.; Greco, A.; Maiorino, A.; Masselli, C. The use of barocaloric effect for energy saving in a domestic refrigerator with ethylene-glycol based nanofluids: A numerical analysis and a comparison with a vapor com-pression cooler. *Energy* **2020**, *190*, 116404. [CrossRef]

57. Liu, J.; Li, Z.; Liu, H.; Yu, L.; Zhang, Y.; Cao, Y.; Xu, K.; Liu, Y. Martensitic Transformation and Barocaloric Effect in Co-V-Ga-Fe Paramagnetic Heusler Alloy. *Metals* **2022**, *12*, 516. [CrossRef]

58. Moya, X.; Defay, E.; Heine, V.; Mathur, N.D. Too cool to work. *Nat. Phys.* **2015**, *11*, 202–205. [CrossRef]

59. Moya, X.; Kar-Narayan, S.; Mathur, N.D. Caloric materials near ferroic phase transitions. *Nat. Mater.* **2014**, *13*, 439–450. [CrossRef] [PubMed]

60. Czernuszewicz, A.; Kaleta, J.; Lewandowski, D.; Przybylski, M. An idea of the test stand for studies of mag-netobarocaloric materials properties and possibilities of their application. *Phys. Status Solidi C Curr. Top. Solid State Phys.* **2014**, *11*, 995–999. [CrossRef]

61. Czernuszewicz, A.; Kaleta, J.; Królewicz, M.; Lewandowski, D.; Mech, R.; Wiewiórski, P. A test stand to study the possibility of using magnetocaloric materials for refrigerators. *Int. J. Refrig.* **2014**, *37*, 72–77. [CrossRef]

62. Aprea, C.; Greco, A.; Maiorino, A.; Masselli, C. Solid-state refrigeration: A comparison of the energy perfor-mances of caloric materials operating in an active caloric regenerator. *Energy* **2018**, *165*, 439–455. [CrossRef]

63. Imamura, W.; Usuda, O.; Paixão, L.S.; Bom, N.M.; Gomes, A.M.; Carvalho, A.M.G. Supergiant Barocaloric Effects in Acetoxy Silicone Rubber over a Wide Temperature Range: Great Potential for Solid-state Cooling. *Chin. J. Polym. Sci.* **2020**, *38*, 999–1005. [CrossRef]

64. Shit, S.C.; Shah, P. A review on silicone rubber. *Natl. Acad. Sci. Lett.* **2013**, *36*, 355–365. [CrossRef]

65. Guo, Y. Investigation of Silicone Rubber Blends and Their Shape Memory Properties. Ph.D. Thesis, University of Akron, Akron, OH, USA, 2018.

66. Halim, Z.A.A.; Ahmad, N.; Yajid, M.A.M.; Hamdan, H. Thermal insulation performance of silicone rubber/silica aerogel composite. *Mater. Chem. Phys.* **2022**, *276*, 125359. [CrossRef]

67. DECRETO LEGISLATIVO 27 gennaio 1992, n. 110. Attuazione Della Direttiva n. 89/108/CEE in Materia di Ali-menti Surgelati destinati All'alimentazione Umana. Decreto del Presidente Della Repubblica. Available online: https://www.gazzettaufficiale.it/atto/serie_generale/caricaDettaglioAtto/originario?atto.dataPubblicazioneGazzetta=1992-02-17&atto.codiceRedazionale=092G0147 (accessed on 30 July 2023).

68. Sebald, G.; Xie, Z.; Guyomar, D. Fatigue effect of elastocaloric properties in natural rubber. *Philos. Trans. R. Soc. A Math. Phys. Eng. Sci.* **2016**, *374*, 20150302. [CrossRef] [PubMed]

69. Woo, C.-S.; Kim, W.-D.; Lee, S.-H.; Choi, B.-I.; Park, H.-S. Fatigue life prediction of vulcanized natural rubber subjected to heat-aging. *Procedia Eng.* **2009**, *1*, 9–12. [CrossRef]

70. Boyer, F.; Fabrie, P. *Mathematical Tools for the Study of the Incompressible Navier-Stokes Equations and Related Models*; Springer Science & Business Media: Berlin/Heidelberg, Germany, 2012; Volume 183.